Supporting Information for

Multilayered ordered protein arrays self-assembled from a mixed population of virus-like particles

Masaki Uchida[1, 2#], Nicholas E. Brunk[3,4,5#], Nathasha D. Hewagama[2], Byeongdu Lee[6], Peter E. Prevelige Jr.[7], Vikram Jadhao[3*], Trevor Douglas[2*]

1. Department of Chemistry and Biochemistry, California State University, Fresno, 2555 E. San Ramon Ave., Fresno, CA 93740, USA
2. Department of Chemistry, Indiana University, 800 E. Kirkwood Ave., Bloomington, IN 47405, USA
3. Intelligent Systems Engineering, Indiana University, 700 N. Woodlawn Ave., Bloomington, IN 47408, USA
4. Wolfram Research, 100 Trade Center Dr., Champaign, IL 61820, USA
5. VeriSIM Life Inc., 1 Sansome St., Suite 3500, San Francisco, CA 94104, USA
6. X-ray science division, Advanced Photon Source, Argonne National Laboratory, 9700 South Cass Ave., Argonne, IL 60439, USA
7. Department of Microbiology, University of Alabama at Birmingham, Birmingham, Alabama 35294, USA

[#] Contributed equally to this work

* Corresponding author:
Trevor Douglas
Department of Chemistry, Indiana University
800 E. Kirkwood Ave., Bloomington, IN 47405
Phone: (812) 856-6936
Fax: (812) 856-5710
Email: trevdoug@iu.edu

Vikram Jadhao
Intelligent Systems Engineering, Indiana University
700 N. Woodlawn Ave., Bloomington, IN 47408, USA
Phone: (812) 856-4018
Email: vjadhao@iu.edu

Table of Contents

Section 1: Experimental details of P22 VLP purification and characterization

Materials

DNA primers were purchased from Eurofins MWG Operon (Huntsville, AL) and Integrated DNA Technologies (Coralville, IA). *E. coli* BL21(DE3) strain and 10G strain were purchased from Lucigen (Madison, WI). QIAprep Spin Miniprep kit were purchased from Qiagen (Valencia, CA). DNase, RNase, lysozyme, and PAMAM dendrimers were purchased from Sigma Aldrich (St. Louis, MO). Alexa Fluor 488 C_5 maleimide and Texas Red C_2 maleimide were purchased from Invitrogen (Waltham, MA). CF 405M maleimide was purchased from Biotium (Fremont, CA). All other chemical reagents were purchased from Fisher Scientific (Pittsburgh, PA). DNA sequences of the proteins used in this study are summarized in section 2 of the supplementary information. All water was deionized using a Milli-Q Advantage A10 water purification system (EMD Millipore).

Genetic engineering, expression and purification of P22 VLP mutants

The P22 VLP is composed of 420 copies of a coat protein (CP) that assembles into a $T = 7$, 56 nm icosahedral capsid with the aid of approximately 100 – 300 copies of a scaffolding protein (SP).[1-2] A truncated form of SP (amino acids 142 to 303, hereafter referred to as SP_{141}) and a CP were cloned into the first and the second multiple cloning sites of the pRSFDuet-1 vector (Novagen), respectively. Two repeats of various heptapeptide sequences were introduced at the C-terminus of the CP (hereafter referred to as CP-EEE2, CP-E2, CP-Q2, and CP-K2). The P22 VLPs with the EEE2 peptide, E2 peptide, Q2 peptide, and the K2 peptide are referred to as P22-EEE2, P22-E2, P22-Q2, and P22-K2, respectively. Each pRSFDuet-1 vector containing either CP-EEE2, CP-E2, CP-Q2, or CP-K2 together with SP_{141} genes, was transformed into BL21(DE3) *E. coli* strain. Each type of P22 variants was purified from *E. coli* with a phosphate

buffer (sodium phosphate 50 mM, sodium chloride 100 mM, pH 7.0, hereafter referred to as standard phosphate buffer) using an established protocol described elsewhere.[3-4]

Characterization of P22 VLPs

The overall morphology of the purified P22 VLPs was analyzed with transmission electron microscopy (TEM; JEM 1010 transmission electron microscope, JEOL Ltd., Akishima, Japan). Hydrodynamic diameter of the VLPs were analyzed with Zetasizer Nano ZS (Malvern Instruments, Worcestershire, UK). Zeta-potential of VLPs in a phosphate buffer (sodium phosphate 10 mM, sodium chloride 20 mM, pH 7.0) was measured with Zetasizer Nano ZS. The Smoluchowski approximation was used to convert the electrophoretic mobility to zeta-potential. The concentration of P22 VLPs was determined by UV absorbance at 280 nm (Agilent 8543). Molecular weights of the four CP mutants with three different peptides were analyzed with ESI-Q-TOF mass spectrometry (Synapt G2S, Waters, Milford, MA) interfaced to an Acquity ultra performance liquid chromatography (UPLC; Waters) equipped with a reverse phase column (Jupiter C4 5μm 300 Å, Phenomenex) as described elsewhere.[5]

PAMAM G6 dendrimer mediated assembly of individual types of VLPs was first assessed by the increase in turbidity upon mixing the solutions of the VLP and the dendrimer (Fig 1b in the main text). Each type of VLP was buffer exchanged to phosphate buffer solutions with various ionic strengths. PAMAM G6 dendrimer in methanol (as purchased) was diluted with the same buffer solutions at a ratio of 1:4 (v/v). A volume of 150 μL of P22 VLP (50 nM VLP) in a phosphate buffer solution was mixed with the dendrimer solution of the same buffer at the ratio of 1000 dendrimer / VLP. The increase in optical density of the sample solution at 800 nm was measured on a UV-Vis spectrometer (Agilent 8453) 30 min after mixing with the dendrimers.

Labeling of P22 VLPs with fluorescence molecules

Each type of P22 VLPs was conjugated with a fluorescence molecule at cysteines in SPs, which were incorporated inside of the VLPs. P22-EEE2 and P22-K2 VLPs were labeled with Alexa Fluor 488 C_5 maleimide. P22-E2 was labeled with Texas Red C_2 maleimide. P22-Q2 was labeled with CF 405M maleimide. Prior to the conjugation reaction, P22 VLPs were incubated with 1 mM DTT in standard phosphate buffer at room temperature for 2 h with gentle shaking. DTT was then removed by two cycles of ultracentrifugation to pellet down P22 VLPs followed by resuspension in the phosphate buffer.

Concentration of P22 VLPs was adjusted to around 1 – 2 mg/mL in standard phosphate buffer. Fluorescence molecules were dissolved in DMSO to a concentration of 10 mM. P22 VLPs were incubated with fluorescent molecules at room temperature for 4 h on a rocker. Ratio of dye/SP was varied with the type of dye molecules. It was 0.3, 0.5, and 1.5 for Texas Red, Alexa Fluor 488, and CF 405M, respectively. After the labeling reaction, unreacted maleimide was quenched by adding 50 equivalents of 2-mercaptoethanol per dye. Unreacted dye and 2-mercaptoethanol were removed by two cycles of ultracentrifugation followed by resuspension of P22 VLPs in phosphate buffer.

Estimation of threshold ionic strength

The threshold ionic strength (I_t) value, below which VLPs of that variant assembly into arrays, was estimated based on the changes in the turbidity of the VLP solution when mixed with G6 dendrimer solutions at different ionic strengths (Table 1 of the main paper). Four individual samples of the same variant were subjected to the turbidity measurement monitoring the optical density at 800 nm with an UV-Vis spectroscopy (Agilent 8453) at each ionic strength 30 min after the addition of the dendrimer. Within the range of ionic strength values examined, there

was a significant difference in optical density for all four P22 variants between the solution of the highest ionic strength at which that variant still assembled into arrays and the next higher ionic strength. For example, higher-order assembly of P22-EEE2 was examined at $I = 535$, 555, and 576 mM (i.e. ≈ 20 mM increment) besides other lower and higher ionic strengths. All sample solutions at $I = 535$ and 555 mM showed drastic increase in optical density, indicating that P22-EEE2 VLPs assembled into arrays. On the other hands, solutions at $I = 576$ mM showed almost no increase. Based on these results, I_t of P22-EEE2 was determined as 555 mM with potential viability of ≈ 20 mM.

Estimation of the yield of the two components core-shell assembly

The solutions containing the P22 VLP assemblies with G6 dendrimer at $I = 41$ mM were mixed well by pipetting up and down and gently pelleted down in a table top centrifuge (at 5000 g for 3 mins). A volume of 100 uL of the supernatant was carefully transferred into a cuvette without disturbing the pellet and the UV absorbance at 280 nm was measured (Agilent 8543). This was repeated for three independent assemblies prepared at $I = 41$ mM. The absorbance at 280 nm of the mixture of P22-E2, P22-K2, and G6 dendrimer at $I = 329$ mM was also measured. To estimate the absorbance at 280 nm contributed from the G6 dendrimer, a solution containing the same concentration of G6 dendrimer but no P22 VLPs was prepared at both $I = 329$ mM and $I = 41$ mM and the absorbance at 280 nm of these two solutions was measured. When preparing the assemblies, a ratio of 1000 G6 dendrimer molecules per VLP was used and it was estimated that only 20 - 30 dendrimer molecules per VLP are incorporated into an ordered array.[5] Thus 97-98% of the G6 dendrimers is expected to be present in the supernatant even at $I = 41$ mM. Therefore, the absorbance at 280 nm of the G6 dendrimer at both $I = 329$ mM and $I = 41$ mM conditions at corresponding amounts were subtracted from the total absorbance at 280 nm measured for the

P22 VLP and G6 dendrimer mixtures to get the net absorbance at 280 nm of the P22 VLPs at $I = 329$ mM and in the supernatant at $I = 41$ mM.

The fraction of the net absorbance at 280 nm of the supernatant at $I = 41$ mM compared to that in the solution at $I = 329$ mM was used to estimate the yield of the P22 VLP assembly. The yield of the assembly of arrays is estimated to be 96.77 ± 1.02 %.

Section 2: DNA sequences of proteins used in this study

(DNA sequences corresponding to two repeats of hepta peptides introduced to modulate the surface charge of P22 VLPs are underlined)

CP with EEE2 (CP-EEE2)

ATG GCT TTG AAC GAA GGT CAA ATT GTT ACA CTG GCG GTA GAT GAA ATC ATC GAA ACC ATC TCC
GCA ATC ACT CCA ATG GCG CAG AAA GCC AAG AAA TAC ACC CCG CCT GCT GCT TCT ATG CAG CGC
TCC AGC AAT ACC ATC TGG ATG CCT GTA GAG CAA GAG TCA CCC ACT CAG GAG GGC TGG GAT TTA
ACT GAT AAA GCG ACA GGG TTA CTG GAA CTT AAC GTC GCG GTA AAC ATG GGA GAG CCG GAT AAC
GAC TTC TTC CAG TTG CGT GCT GAT GAC TTG CGA GAC GAA ACT GCG TAT CGT CGC CGC ATC CAG
TCT GCC GCT CGC AAG CTG GCG AAC AAC GTT GAG TTG AAA GTC GCA AAC ATG GCC GCC GAG ATG
GGT TCG CTG GTT ATC ACC TCC CCT GAT GCC ATC GGC ACT AAT ACC GCA GAC GCC TGG AAC TTT
GTG GCC GAC GCA GAA GAA ATC ATG TTC TCC CGC GAA CTT AAC CGC GAC ATG GGG ACA TCG TAC
TTC TTC AAC CCT CAG GAC TAC AAA AAA GCG GGT TAC GAC CTG ACC AAG CGT GAC ATC TTC GGG
CGT ATT CCT GAA GAA GCA TAC CGA GAT GGC ACC ATT CAG CGT CAG GTC GCT GGC TTC GAT GAT
GTC CTG CGC TCT CCG AAA CTT CCT GTG CTG ACC AAA TCC ACC GCA ACT GGC ATC ACT GTA TCC
GGT GCG CAG TCC TTC AAG CCT GTC GCA TGG CAA CTG GAT AAC GAT GGC AAC AAA GTT AAC GTT
GAT AAC CGT TTT GCT ACC GTC ACC CTG TCT GCA ACT ACC GGC ATG AAA CGC GGC GAC AAA ATT
TCG TTT GCT GGC GTT AAG TTC CTT GGT CAG ATG GCT AAG AAC GTA CTG GCT CAG GAT GCG ACT
TTC TCC GTA GTC CGC GTT GTT GAC GGT ACT CAT GTT GAA ATC ACG CCG AAG CCG GTA GCG CTG
GAT GAT GTT TCC CTG TCT CCG GAG CAG CGT GCC TAC GCC AAC GTT AAC ACC TCG CTG GCT GAT
GCA ATG GCA GTG AAC ATT CTG AAC GTT AAA GAC GCT CGC ACT AAT GTG TTC TGG GCT GAC GAT
GCT ATT CGT ATC GTG TCT CAG CCG ATT CCG GCT AAC CAT GAA CTT TTT GCA GGT ATG AAA ACT
ACC TCA TTC AGC ATC CCT GAT GTT GGC CTG AAC GGT ATC TTC GCT ACG CAG GGT GAT ATT TCC
ACC CTG TCC GGC CTG TGC CGT ATT GCG CTG TGG TAC GGC GTA AAC GCG ACA CGA CCG GAG GCA
ATC GGT GTT GGC CTG CCT GGT CAG ACT GCG ACT AGT GTG GCG GCG CTG GAA GAG GAA GTT GCC
GCC TTG GAG GAG GAG TAG

CP with E2 (CP-E2)

ATG GCT TTG AAC GAA GGT CAA ATT GTT ACA CTG GCG GTA GAT GAA ATC ATC GAA ACC ATC TCC
GCA ATC ACT CCA ATG GCG CAG AAA GCC AAG AAA TAC ACC CCG CCT GCT GCT TCT ATG CAG CGC
TCC AGC AAT ACC ATC TGG ATG CCT GTA GAG CAA GAG TCA CCC ACT CAG GAG GGC TGG GAT TTA
ACT GAT AAA GCG ACA GGG TTA CTG GAA CTT AAC GTC GCG GTA AAC ATG GGA GAG CCG GAT AAC
GAC TTC TTC CAG TTG CGT GCT GAT GAC TTG CGA GAC GAA ACT GCG TAT CGT CGC CGC ATC CAG
TCT GCC GCT CGC AAG CTG GCG AAC AAC GTT GAG TTG AAA GTC GCA AAC ATG GCC GCC GAG ATG
GGT TCG CTG GTT ATC ACC TCC CCT GAT GCC ATC GGC ACT AAT ACC GCA GAC GCC TGG AAC TTT
GTG GCC GAC GCA GAA GAA ATC ATG TTC TCC CGC GAA CTT AAC CGC GAC ATG GGG ACA TCG TAC
TTC TTC AAC CCT CAG GAC TAC AAA AAA GCG GGT TAC GAC CTG ACC AAG CGT GAC ATC TTC GGG
CGT ATT CCT GAA GAA GCA TAC CGA GAT GGC ACC ATT CAG CGT CAG GTC GCT GGC TTC GAT GAT
GTC CTG CGC TCT CCG AAA CTT CCT GTG CTG ACC AAA TCC ACC GCA ACT GGC ATC ACT GTA TCC
GGT GCG CAG TCC TTC AAG CCT GTC GCA TGG CAA CTG GAT AAC GAT GGC AAC AAA GTT AAC GTT
GAT AAC CGT TTT GCT ACC GTC ACC CTG TCT GCA ACT ACC GGC ATG AAA CGC GGC GAC AAA ATT
TCG TTT GCT GGC GTT AAG TTC CTT GGT CAG ATG GCT AAG AAC GTA CTG GCT CAG GAT GCG ACT
TTC TCC GTA GTC CGC GTT GTT GAC GGT ACT CAT GTT GAA ATC ACG CCG AAG CCG GTA GCG CTG
GAT GAT GTT TCC CTG TCT CCG GAG CAG CGT GCC TAC GCC AAC GTT AAC ACC TCG CTG GCT GAT
GCA ATG GCA GTG AAC ATT CTG AAC GTT AAA GAC GCT CGC ACT AAT GTG TTC TGG GCT GAC GAT
GCT ATT CGT ATC GTG TCT CAG CCG ATT CCG GCT AAC CAT GAA CTT TTT GCA GGT ATG AAA ACT
ACC TCA TTC AGC ATC CCT GAT GTT GGC CTG AAC GGT ATC TTC GCT ACG CAG GGT GAT ATT TCC
ACC CTG TCC GGC CTG TGC CGT ATT GCG CTG TGG TAC GGC GTA AAC GCG ACA CGA CCG GAG GCA
ATC GGT GTT GGC CTG CCT GGT CAG ACT GCG ACT AGT GTG GCG GCG CTG GAA AAA GAA GTT GCC
GCC TTG GAG AAG GAG TAG

CP with Q2 (CP-Q2)

ATG GCT TTG AAC GAA GGT CAA ATT GTT ACA CTG GCG GTA GAT GAA ATC ATC GAA ACC ATC TCC
GCA ATC ACT CCA ATG GCG CAG AAA GCC AAG AAA TAC ACC CCG CCT GCT GCT TCT ATG CAG CGC
TCC AGC AAT ACC ATC TGG ATG CCT GTA GAG CAA GAG TCA CCC ACT CAG GAG GGC TGG GAT TTA
ACT GAT AAA GCG ACA GGG TTA CTG GAA CTT AAC GTC GCG GTA AAC ATG GGA GAG CCG GAT AAC
GAC TTC TTC CAG TTG CGT GCT GAT GAC TTG CGA GAC GAA ACT GCG TAT CGT CGC CGC ATC CAG
TCT GCC GCT CGC AAG CTG GCG AAC AAC GTT GAG TTG AAA GTC GCA AAC ATG GCC GCC GAG ATG
GGT TCG CTG GTT ATC ACC TCC CCT GAT GCC ATC GGC ACT AAT ACC GCA GAC GCC TGG AAC TTT
GTG GCC GAC GCA GAA GAA ATC ATG TTC TCC CGC GAA CTT AAC CGC GAC ATG GGG ACA TCG TAC

TTC TTC AAC CCT CAG GAC TAC AAA AAA GCG GGT TAC GAC CTG ACC AAG CGT GAC ATC TTC GGG
CGT ATT CCT GAA GAA GCA TAC CGA GAT GGC ACC ATT CAG CGT CAG GTC GCT GGC TTC GAT GAT
GTC CTG CGC TCT CCG AAA CTT CCT GTG CTG ACC AAA TCC ACC GCA ACT GGC ATC ACT GTA TCC
GGT GCG CAG TCC TTC AAG CCT GTC GCA TGG CAA CTG GAT AAC GAT GGC AAC AAA GTT AAC GTT
GAT AAC CGT TTT GCT ACC GTC ACC CTG TCT GCA ACT ACC GGC ATG AAA CGC GGC GAC AAA ATT
TCG TTT GCT GGC GTT AAG TTC CTT GGT CAG ATG GCT AAG AAC GTA CTG GCT CAG GAT GCG ACT
TTC TCC GTA GTC CGC GTT GTT GAC GGT ACT CAT GTT GAA ATC ACG CCG AAG CCG GTA GCG CTG
GAT GAT GTT TCC CTG TCT CCG GAG CAG CGT GCC TAC GCC AAC GTT AAC ACC TCG CTG GCT GAT
GCA ATG GCA GTG AAC ATT CTG AAC GTT AAA GAC GCT CGC ACT AAT GTG TTC TGG GCT GAC GAT
GCT ATT CGT ATC GTG TCT CAG CCG ATT CCG GCT AAC CAT GAA CTT TTT GCA GGT ATG AAA ACT
ACC TCA TTC AGC ATC CCT GAT GTT GGC CTG AAC GGT ATC TTC GCT ACG CAG GGT GAT ATT TCC
ACC CTG TCC GGC CTG TGC CGT ATT GCG CTG TGG TAC GGC GTA AAC GCG ACA CGA CCG GAG GCA
ATC GGT GTT GGC CTG CCT GGT CAG ACT GCG ACT AGT GTG GCG GCG CTG CAG AGC CAA GTG GCG
GCG CTT CAA AGT CAG TAA

CP with K2 (CP-K2)

ATG GCT TTG AAC GAA GGT CAA ATT GTT ACA CTG GCG GTA GAT GAA ATC ATC GAA ACC ATC TCC
GCA ATC ACT CCA ATG GCG CAG AAA GCC AAG AAA TAC ACC CCG CCT GCT GCT TCT ATG CAG CGC
TCC AGC AAT ACC ATC TGG ATG CCT GTA GAG CAA GAG TCA CCC ACT CAG GAG GGC TGG GAT TTA
ACT GAT AAA GCG ACA GGG TTA CTG GAA CTT AAC GTC GCG GTA AAC ATG GGA GAG CCG GAT AAC
GAC TTC TTC CAG TTG CGT GCT GAT GAC TTG CGA GAC GAA ACT GCG TAT CGT CGC CGC ATC CAG
TCT GCC GCT CGC AAG CTG GCG AAC AAC GTT GAG TTG AAA GTC GCA AAC ATG GCC GCC GAG ATG
GGT TCG CTG GTT ATC ACC TCC CCT GAT GCC ATC GGC ACT AAT ACC GCA GAC GCC TGG AAC TTT
GTG GCC GAC GCA GAA GAA ATC ATG TTC TCC CGC GAA CTT AAC CGC GAC ATG GGG ACA TCG TAC
TTC TTC AAC CCT CAG GAC TAC AAA AAA GCG GGT TAC GAC CTG ACC AAG CGT GAC ATC TTC GGG
CGT ATT CCT GAA GAA GCA TAC CGA GAT GGC ACC ATT CAG CGT CAG GTC GCT GGC TTC GAT GAT
GTC CTG CGC TCT CCG AAA CTT CCT GTG CTG ACC AAA TCC ACC GCA ACT GGC ATC ACT GTA TCC
GGT GCG CAG TCC TTC AAG CCT GTC GCA TGG CAA CTG GAT AAC GAT GGC AAC AAA GTT AAC GTT
GAT AAC CGT TTT GCT ACC GTC ACC CTG TCT GCA ACT ACC GGC ATG AAA CGC GGC GAC AAA ATT
TCG TTT GCT GGC GTT AAG TTC CTT GGT CAG ATG GCT AAG AAC GTA CTG GCT CAG GAT GCG ACT
TTC TCC GTA GTC CGC GTT GTT GAC GGT ACT CAT GTT GAA ATC ACG CCG AAG CCG GTA GCG CTG
GAT GAT GTT TCC CTG TCT CCG GAG CAG CGT GCC TAC GCC AAC GTT AAC ACC TCG CTG GCT GAT
GCA ATG GCA GTG AAC ATT CTG AAC GTT AAA GAC GCT CGC ACT AAT GTG TTC TGG GCT GAC GAT
GCT ATT CGT ATC GTG TCT CAG CCG ATT CCG GCT AAC CAT GAA CTT TTT GCA GGT ATG AAA ACT
ACC TCA TTC AGC ATC CCT GAT GTT GGC CTG AAC GGT ATC TTC GCT ACG CAG GGT GAT ATT TCC
ACC CTG TCC GGC CTG TGC CGT ATT GCG CTG TGG TAC GGC GTA AAC GCG ACA CGA CCG GAG GCA
ATC GGT GTT GGC CTG CCT GGT CAG ACT GCG ACT AGG GTG GCG GCG CTG AAA GAA AAA GTT GCC
GCC TTA AAG GAG AAG TAG

SP_{141}

ATG GGC AGC AGC CAT CAC CAT CAT CAC CAC AGC CAG GAT CCC TGG TGC CGC GCG GCA GCA TGT
CGC AGC AAT GCC GTA GCA GAA CAG GGC CGC AAG ACT CAG GAG TTT ACC CAG CAA TCA GCG CAA
TAC GTC GAA GCT GCC CGC AAA CAC TAT GAC GCG GCG GAA AAG CTC AAC ATC CCT GAC TAT CAG
GAG AAA GAA GAC GCA TTT ATG CAA CTG GTT CCG CCT GCG GTT GGG GCC GAC ATT ATG CGC CTG
TTC CCG GAA AAG TCC GCC GCG CTC ATG TAT CAC CTG GGG GCA AAC CCG GAG AAA GCC CGC CAG
TTA CTG GCG ATG GAT GGG CAG TCC GCG CTG ATT GAA CTC ACT CGA CTA TCC GAA CGC TTA ACT
CTC AAG CCT CGC GGT AAA CAA ATC TCT TCC GCT CCC CAT GCT GAC CAG CCT ATT ACC GGT GAT
GTC AGC GCA GCA AAT AAA GAT GCC ATT CGT AAA CAA ATG GAT GCT GCT GCG AGC AAG GGA GAT
GTG GAA ACC TAC CGC AAG CTA AAG GCA AAA CTT AAA GGA ATC CGA TAA

Section 3: Figure in Introduction

Fig S1, which is reproduced from a paper by Foty and Steinberg shows formation of a spatially distinct core-shell structure from a mixture of two populations of cells *in vitro*.[6] A mixture of two populations of cells, which are the same cell type but differ in the expression levels of a cell adhesion protein (N-cadherin), segregated from each other, resulting in the formation of a core-shell structure. The segregation was guided by the reduction of the free energy of adhesion as cells tend to maximize their mutual binding. This result demonstrates that spatial segregation of cells during morphogenesis is not solely due to chronological sequences in the developmental process, highlighting the potential of synthetic approaches to fabricate hierarchically organized structures *via* self-assembly of multiple types of building blocks.

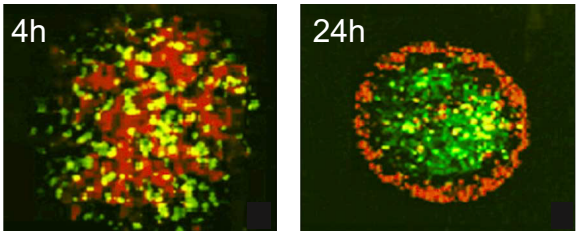

Figure S1: Sorting out of cells differing only in expression level of N-cadherin. Two L cell clones, expressing low and high level of N-cadherin, were labeled with red and green fluorescence dyes, respectively, mixed in equal proportions, and cultured. Confocal optical section through a cell aggregate after 4 h of incubation showed initial mixture of the cells (left). Confocal optical section after 24 h of incubation exhibited segregation of cells. The cells expressing lower level of N-cadherin segregated from and enveloped the cells expressing higher level of N-cadherin, resulting in the formation of a core-shell morphology (right). Reproduced with permission from ref 6. Copyright 2005 Elsevier.

Section 4: Characterization of P22 VLPs

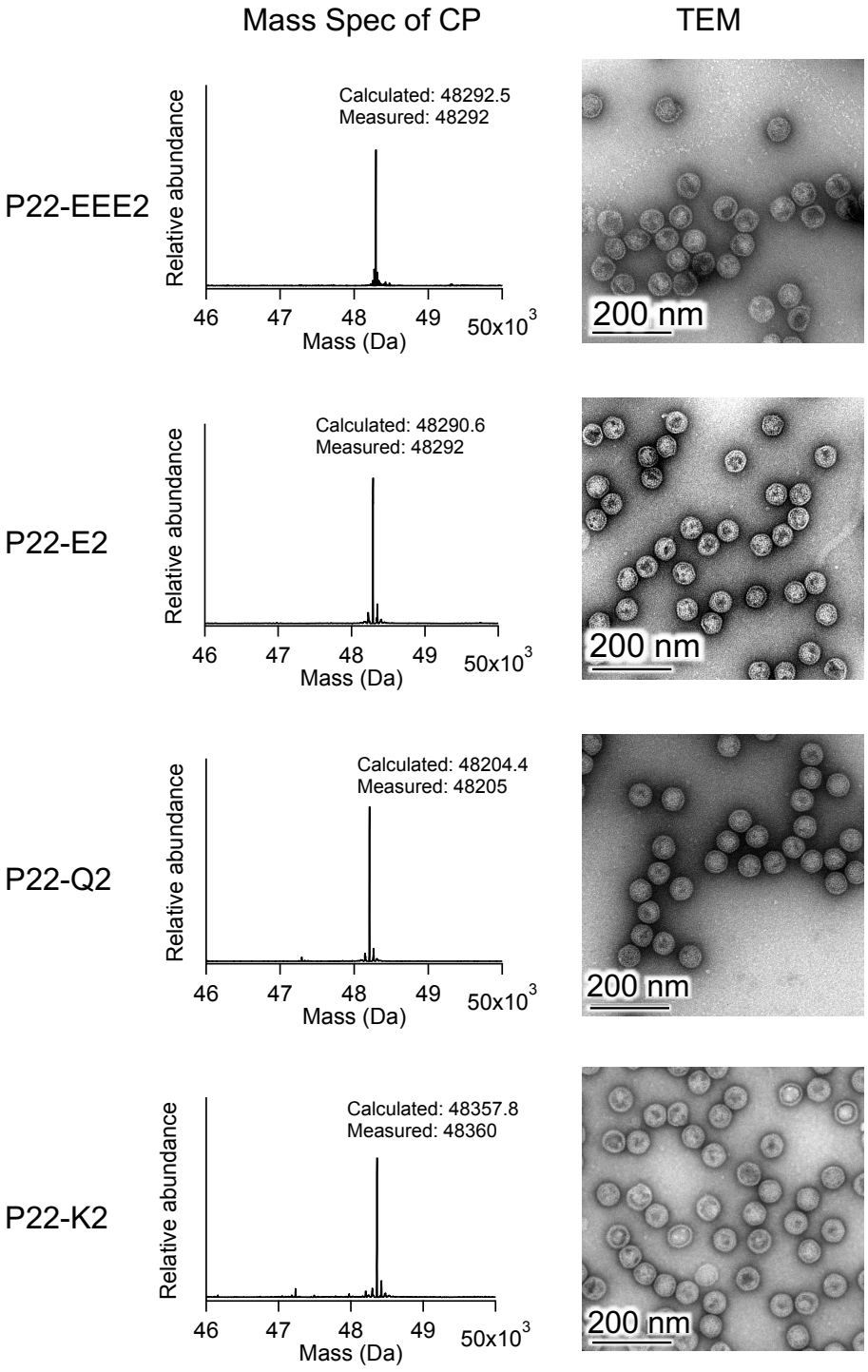

Figure S2: Characterization of P22 VLPs. Left: Deconvoluted mass analyses of coat protein (CP) mutants. The measured molecular weights of all four CP variants were matched well with the calculated molecular weights. Right: TEM images of P22 VLPs. All four types of P22 VLPs showed capsid structures with diameters of about 55 nm regardless of the modifications to the CP.

Section 5: Additional SIM images

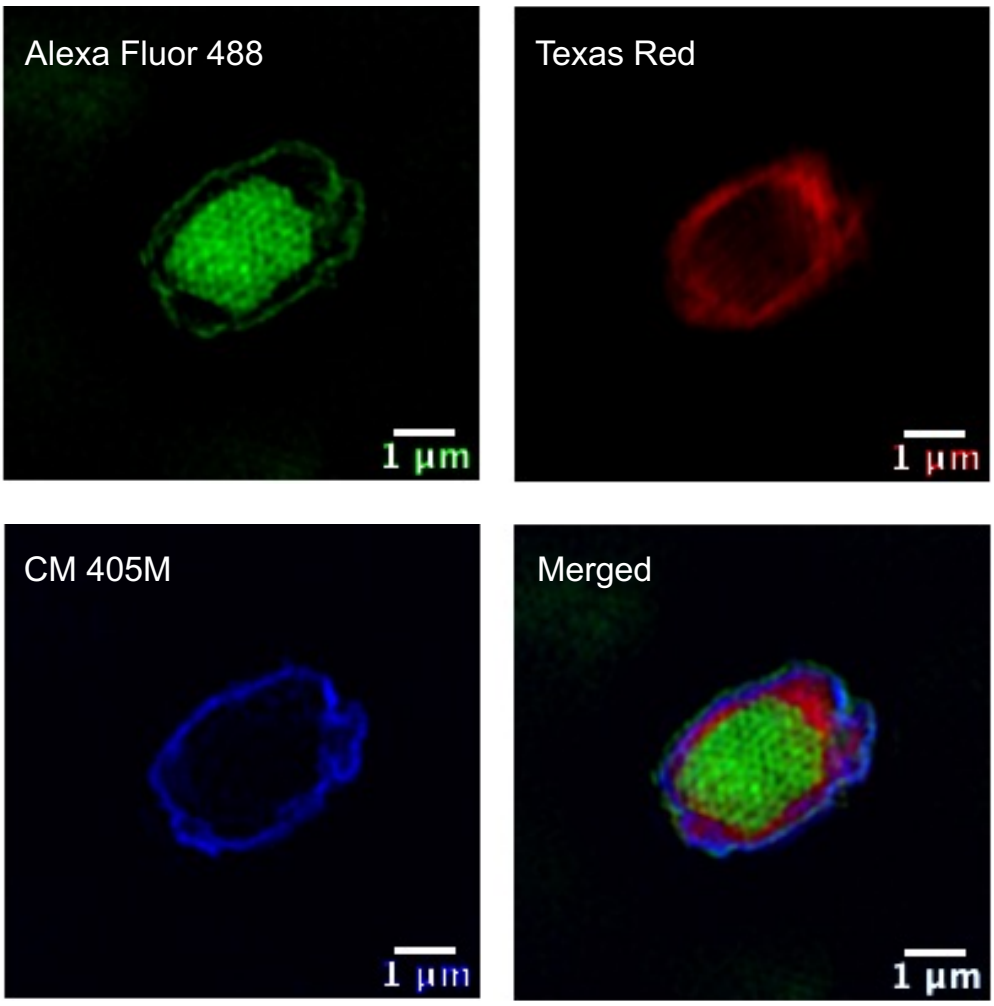

Figure S3: Super-resolution 3D-SIM images of the array sample self-assembled from mixed four types of P22 VLPs through a step-by-step dialysis from $I = 823$ mM to 41 mM. Images of individual channel as well as the merged image shows that P22-EEE2 VLPs (labeled with Alexa Fluor 488), P22-E2 VLPs (labeled with Texas Red), P22-Q2 VLPs (labeled with CM 405M), and P22-K2 VLPs (labeled with Alexa Fluor 488) assembled into distinct spatially segregated layers, leading to the four-layered array formation.

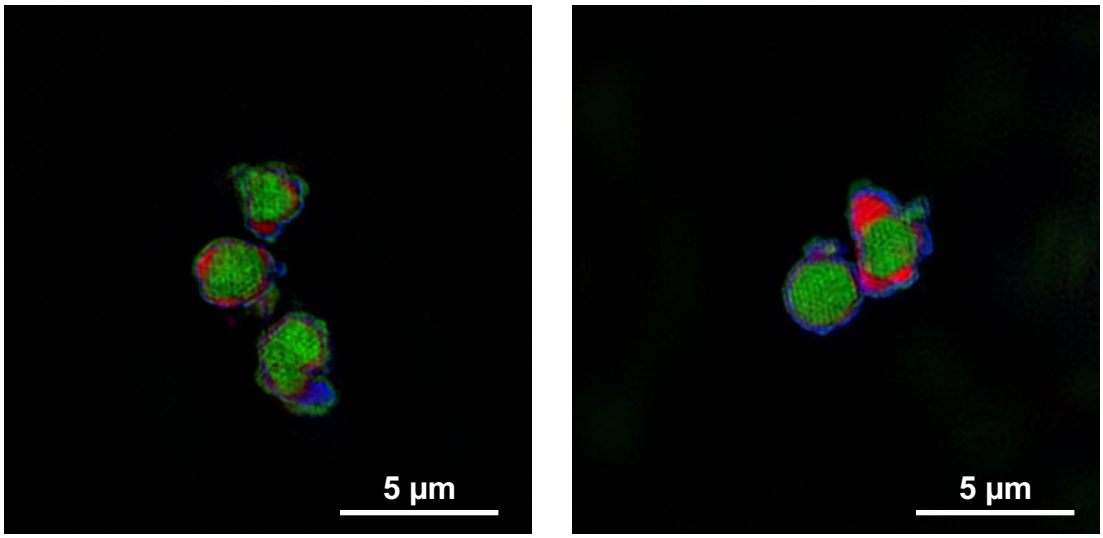

Figure S4: Additional super-resolution fluorescence microscopy images of P22 VLP arrays formed in a mixture of four types of VLPs after step-by-step dialysis from the ionic strength I = 823 mM to 41 mM. P22-EEE2, P22-E2, P22-Q2, and P22-K2 VLPs were labeled with Alexa-488, Texas Red, CF405M, and Alexa-488 fluorescent dyes, respectively.

Section 6: Structure analysis of SAXS data obtained from four components core-shell sample

The peak positions of prominent peaks observed from the four-layered core-shell array obtained at $I = 41$ mM were nearly identical to those of previously reported P22-E2 VLP arrays with an FCC structure[4-5]. The lattice parameter a of the FCC structure was deduced with the following equation:

$$\sqrt{h^2 + k^2 + l^2} = \frac{a}{2\pi} q_{hkl}$$

Where h, k, and l are Miller indices of a peak and q_{hkl} is the scattering vector of the peak (Fig S5a and b).

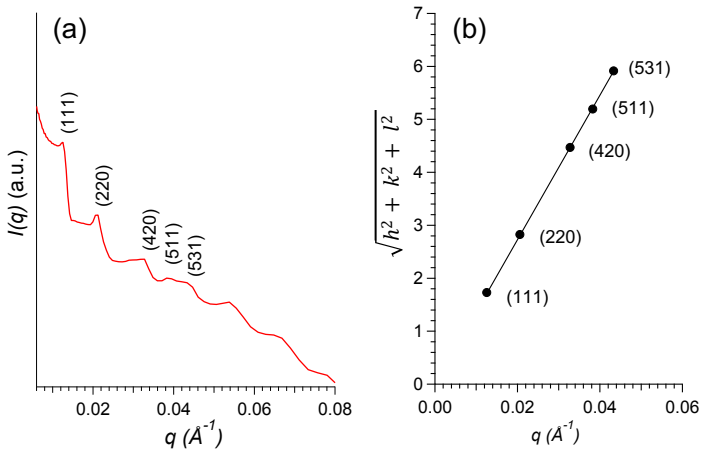

Figure S5: (a) Indexed SAXS profile measured from the four-layered core-shell array obtained at $I = 41$ mM. (b) Quadratic Miller indices of assigned reflections for the FCC structures versus measured scattering vector positions for indexed peaks. The lattice parameter a is estimated as 86.0 nm.

Section 7: Additional computational and experimental data for two-component VLP system and K2-only VLP system

Large field of view fluorescence image of core-shell arrays

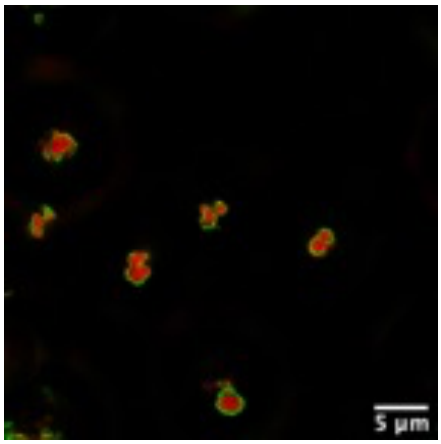

Figure S6: Super-resolution fluorescence microscopy images of P22 VLP arrays formed in a mixture of P22-E2 and P22-K2 VLPs after step-by-step dialysis from the ionic strength I = 329 mM to 41 mM. P22- P22-E2 and P22-K2 VLPs were labeled with Texas Red and Alexa-488 fluorescent dyes, respectively.

Fluorescence image of core-shell arrays stored at 4˚C for 17 months

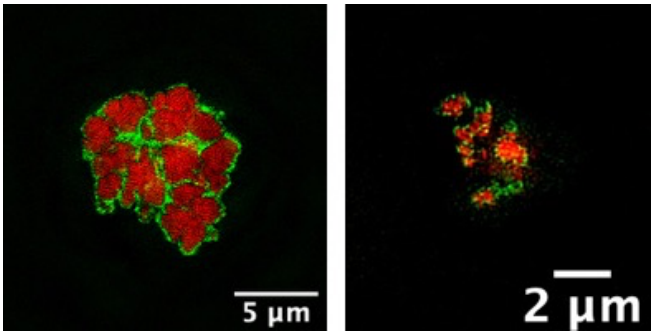

Figure S7: High resolution fluorescence microcopy observation of the core-shell arrays stored at 4˚C for 17 months after the preparation. Over this timeframe, the core-shell architecture is maintained and at least some arrays coalesce.

Cross-section of the two-component core-shell arrays formed in simulations

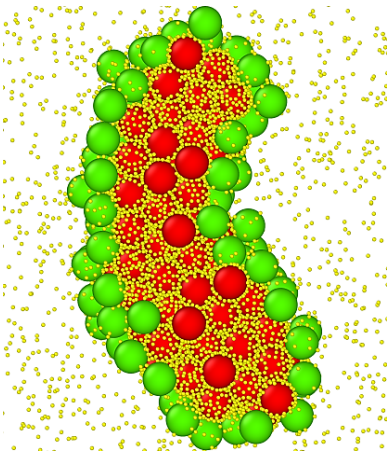

Figure S8: Cross-section of a core-shell array formed in simulations by P22-E2 VLPs (red spheres) and P22-K2 VLPs (green spheres) at an ionic strength of 100 mM. P22-E2 VLPs and P22-K2 VLPs form the core and layer (shell) respectively. The smaller yellow spheres are the dendrimers.

Coarse-grained model of assembly and disassembly of E2-K2 core-shell VLP arrays

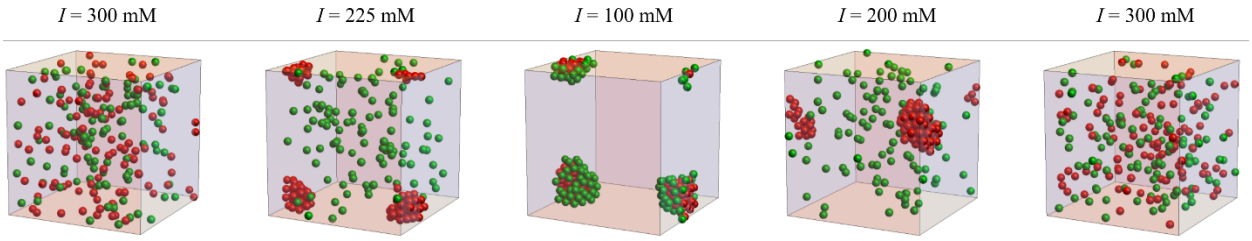

Figure S9: Selected simulation snapshots of a typical steady-state configuration of P22-E2 VLPs (red spheres) and P22-K2 VLPs (green spheres) at different ionic strengths indicated by the legend at the top. Ionic strength decreases from left to right (first 3 snapshots from the left) and then increases (next 2 snapshots). Snapshots illustrate ionic-strength-dependent reversible assembly and disassembly of the two-component VLP system into core-shell structures. No assembly is observed at high ionic strength $I = 300$ mM (left). Exclusive assembly of E2 VLPs occurs at its ionic strength threshold $I_t^{E2} = 225$ mM $\gg I_t^{K2}$, resulting in the formation of the E2 VLP cores (center left). Co-assembly of K2 VLPs on the surface of the E2 VLP cores occurs upon further dialysis to $I = 100$ mM, yielding the formation of shells around the cores (center). When the ionic strength is increased back to $I = 200$ mM $\gg I_t^{K2}$, the K2 VLP layers come off from the E2 VLP cores, yielding dispersed K2 VLPs in the solution (center right). The E2 cores are disassembled into individual VLPs when ionic strength is further increased to $I = 300$ mM $\gg I_t^{E2}$ (right).

Fluorescence images of K2 only assembly through dialysis

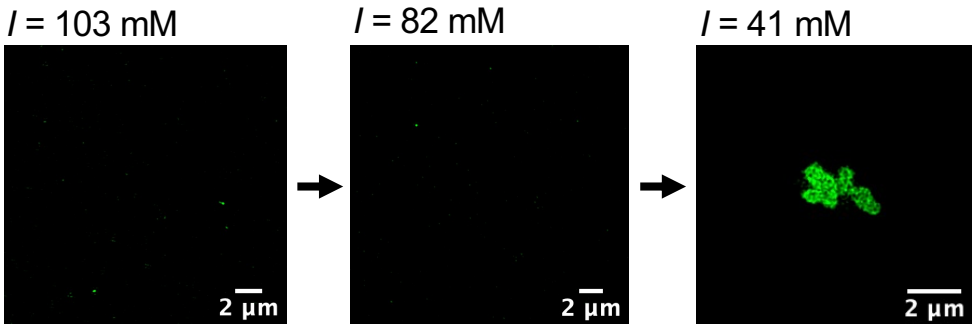

Figure S10: High resolution fluorescence microcopy observation of samples containing only P22-K2 VLPs through the dialysis process. Unlike the samples of the two-component mixture containing P22-E2 and P22-K2 VLPs, in the single-component system, P22-K2 VLPs did not assemble at $I =$ 103 mM, and only showed assembly at $I =$ 41 mM.

Section 8: Condensed and bridging dendrimers

Assembly of P22 VLPs into arrays was mediated by G6 dendrimers. Condensed dendrimer is defined as a dendrimer that is bound to the P22 VLP surface. Bridging dendrimer is defined as a condensed dendrimer that is shared between two VLPs. The average number of condensed and bridging dendrimers were extracted in simulations for different ionic strength of the solution containing P22-E2 VLPs, P22-K2 VLPs (1:1 stoichiometry), and G6 dendrimers (Fig S11). The number of condensed and bridging dendrimers gradually increased as the ionic strength was lowered *via* dialysis. On re-adding salt (increasing ionic strength), the number of condensed and bridging dendrimers decreased. These changes in the number of condensed and bridging dendrimers (linkers) on the VLPs correlate with the observed ionic-strength-modulated reversible assembly and disassembly of the core-shell VLP arrays. Additionally, the enhanced condensation of dendrimers on the surface of the already formed P22-E2 VLP array (Fig S12) enables the P22-E2 VLP core to recruit P22-K2 VLPs to populate the K2 VLP layer at ionic strengths higher than the threshold ionic strength of the single-component P22-K2 VLP system (Fig 2 in the main text).

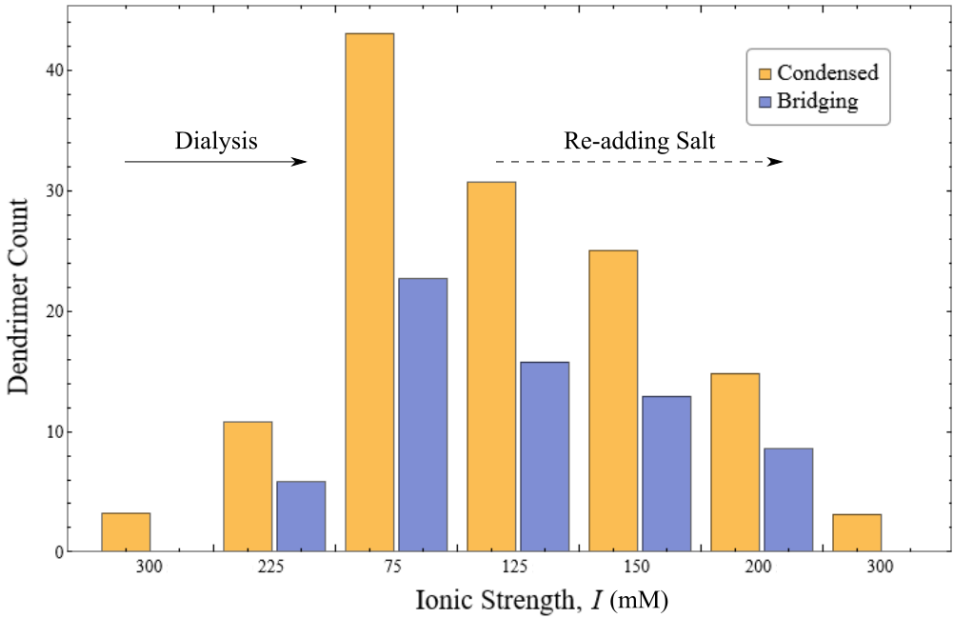

Figure S11: The average number of condensed dendrimers (orange) and bridging dendrimers (blue) per VLP extracted *via* simulations as the ionic strength is first gradually decreased from $I = 300$ mM to 75 mM, and then increased back to 300 mM. The number of condensed and bridging dendrimer increase with decreasing ionic strength, and then decrease with increasing ionic strength.

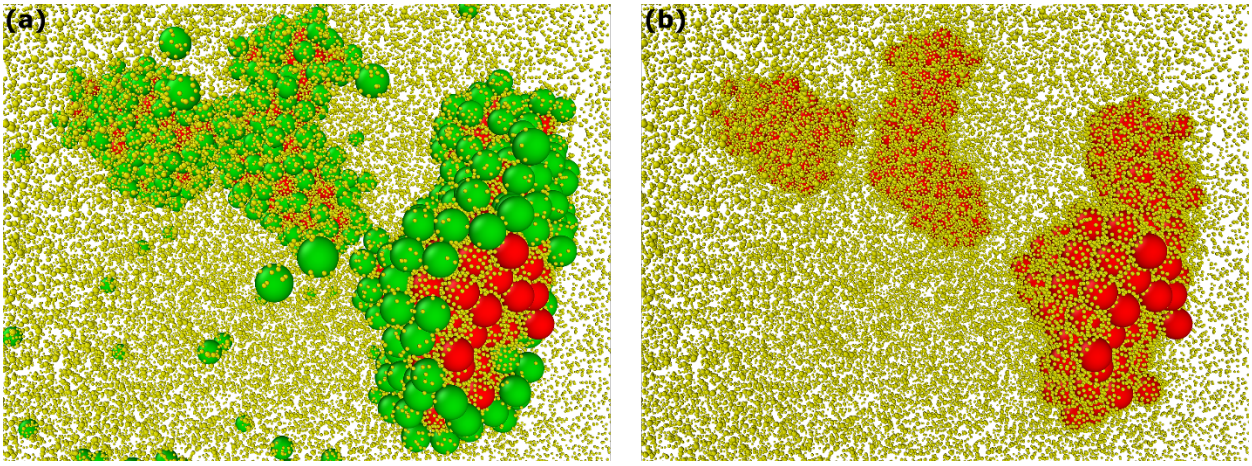

Figure S12: (a) Simulation snapshot of the core-shell structures formed at an ionic strength of 100 mM showing layers of P22-K2 VLPs (green spheres) surrounding the cores made of P22-E2 VLPs (red spheres). The smaller yellow spheres are the dendrimers. (b) The same snapshot with K2 VLPs removed to reveal the surface of the E2 VLPs. Large accumulation of dendrimers is evident on the surface of the E2 VLP core.

Section 9: Lattice contraction observed in dialysis to low ionic strength

In the SAXS profiles of the sample containing both P22-E2 and P22-K2 VLPs, peaks attributed to the structure factor of the ordered VLP array shifted to higher q (*i.e.* corresponding to smaller interplanar distance) when the sample solution was dialyzed from $I = 206$ to 41 mM (Fig S13a). The lattice parameter of the FCC array estimated from the peak position was 88.6 nm at $I = 206$ mM and contracted to 86.3 nm at $I = 41$ mM. This trend was reversible and the peak position shifted back to the initial position when the sample was dialyzed from $I = 41$ mM back up to $I =$ 206 mM. This contraction was not due to the formation of the core-shell structure because the arrays composed of the single-component P22-E2 VLPs also exhibited the tightening of the lattice at $I = 41$ mM (Fig S13b). The Debye screening length, which is the distance over which electrostatic interactions between particles become attenuated in solution, increase with decreasing ionic strength. The observed contraction of the lattice can thus be attributed to the stronger electrostatic attraction between negatively charged VLPs and positively charged G6 dendrimers at lower ionic strengths.

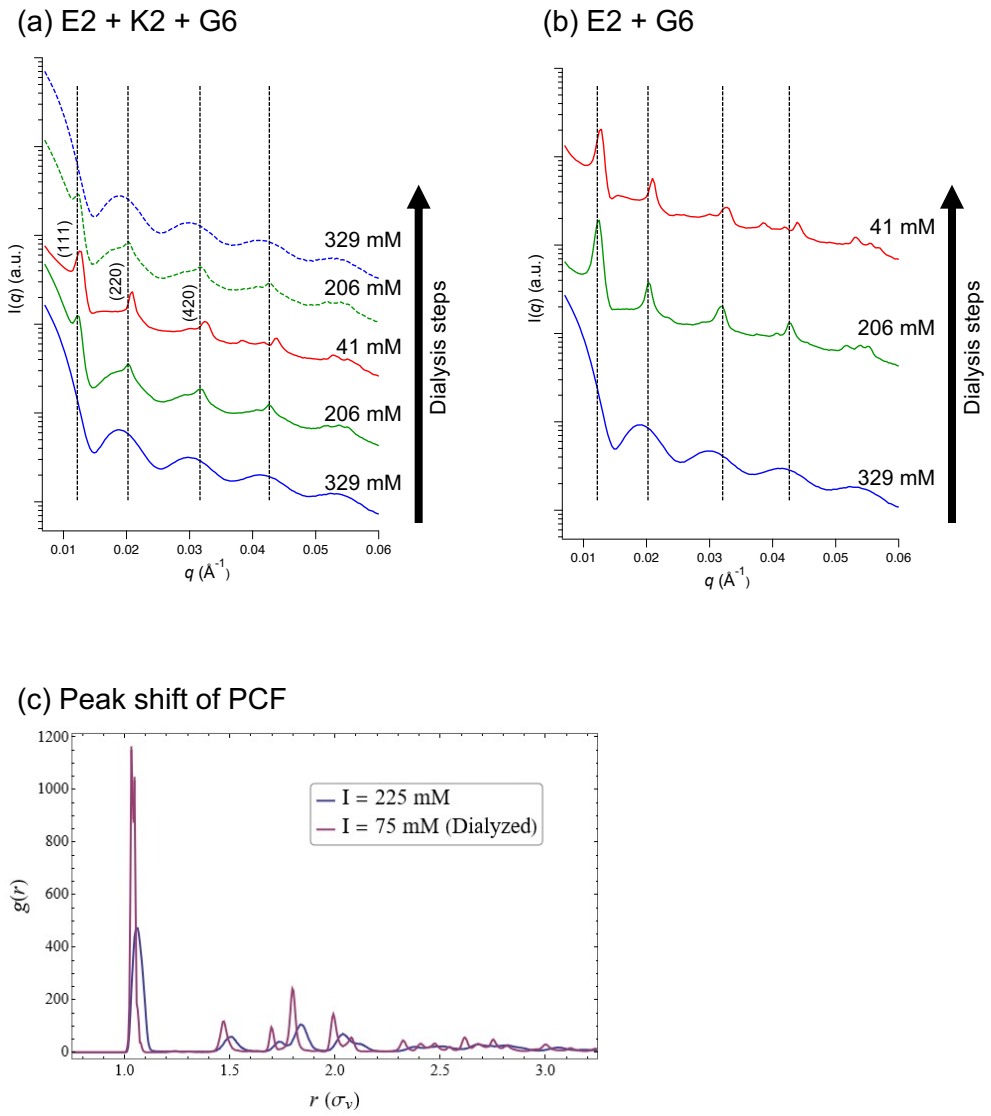

Figure S13: SAXS profiles of samples containing (a) both P22-E2 and P22-K2 VLPs and (b) only P22-E2 VLPs at each step of the dialysis process. The profiles indicate that the assembled arrays have a face centered cubic (FCC) structure. A shift in peak positions to higher q was observed (vertical dashed lines) when the sample containing both E2 and K2 VLPs was dialyzed from $I = 206$ to 41 mM. These peak shifts correspond to a decrease in the lattice parameter from 886.3 Å to 862.7 Å. When the mixture was dialyzed back to 206 mM, the peak positions were restored. Similar peak shift was observed in the case of the single-component E2-only sample as well. (c) Pair correlation functions (PCFs) are shown for the assembly of the single-component system with P22-E2 VLPs in the presence of dendrimers. Results are shown for assembly achieved *via* rapid dilution at an ionic strength $I = 225$ mM, slightly below the ionic strength threshold I_t^{E2} (blue), and assembly achieved *via* dialysis to an ionic strength of $I = 75$ mM well below the threshold (purple). PCF corresponding to the assembled structure achieved *via* dialysis to $I = 75$ mM exhibits sharper peaks and more of them, indicating a higher degree of order, compared to the PCF associated with the structure achieved *via* rapid dilution to $I = 225$ mM. Further, the PCF peaks corresponding to assembled structure achieved at $I = 75$ mM shift to lower *r*, suggesting the contraction of the interparticle distances and the associated lattice structure.

References

(1) Botstein, D.; Waddell, C. H.; King, J., Mechanism of Head Assembly and DNA Encapsulation in Salmonella Phage P22. I. Genes, Proteins, Structures and DNA Maturation. *J Mol Biol* **1973,** *80*, 669-695.

(2) Prevelige, P. E.; Thomas, D.; King, J., Scaffolding Protein Regulates the Polymerization of P22 Coat Subunits into Icosahedral Shells in Vitro. *J Mol Biol* **1988,** *202*, 743-757.

(3) Kang, S.; Uchida, M.; O'Neil, A.; Li, R.; Prevelige, P. E.; Douglas, T., Implementation of P22 Viral Capsids as Nanoplatforms. *Biomacromolecules* **2010,** *11*, 2804-2809.

(4) Uchida, M.; McCoy, K.; Fukuto, M.; Yang, L.; Yoshimura, H.; Miettinen, H. M.; Lafrance, B.; Patterson, D. P.; Schwarz, B.; Karty, J. A.*, et al.*, Modular Self-Assembly of Protein Cage Lattices for Multistep Catalysis. *ACS Nano* **2018,** *12*, 942-953.

(5) Brunk, N. E.; Uchida, M.; Lee, B.; Fukuto, M.; Yang, L.; Douglas, T.; Jadhao, V., Linker-Mediated Assembly of Virus-Like Particles into Ordered Arrays Via Electrostatic Control. *ACS Applied Bio Materials* **2019,** *2*, 2192-2201.

(6) Foty, R. A.; Steinberg, M. S., The Differential Adhesion Hypothesis: A Direct Evaluation. *Dev Biol* **2005,** *278*, 255-263.